RSC Advances

PAPER

View Article Online
View Journal | View Issue

Cite this: *RSC Adv.*, 2015, **5**, 19955

Received 26th December 2014
Accepted 3rd February 2015

DOI: 10.1039/c4ra17065b

www.rsc.org/advances

Growth mechanism of curved Mg–Al–CO_3 layered double hydroxide nanostructures in a one-pot assembly procedure under ambient pressure

Xinxin Zhao, Chenggang Zhou,* Bo Han, Zhuan Ji, Liang Wang and Jinping Wu*

We show that the amount of peroxide added is a governing factor, leading to the curved or amorphous morphologies of Mg–Al-LDH products in a reflux system under ambient pressure. A concerted growth mechanism is proposed to elucidate the formation of the unconventional nano-features of the products.

Introduction

Layered double hydroxides (LDHs), with the general formula of $[M_{1-x}^{2+}M_x^{3+}(OH)_2]A_{x/n}^{n-}\cdot mH_2O$, are composed of the layered planar sheets of M^{2+}/M^{3+} hydroxides and the interlayer of A^{n-} anions.[1–8] By assembling functional agents to the delaminated LDHs,[9–12] a broad variety of applications may be developed, including polymer/LDH nanocomposites,[13–21] functional thin films,[22–25] catalysts,[26,27] electrode materials,[28–33] photo-functional materials[34,35] and bioinorganic hybrid materials.[36] Thus, an appropriate and simple delamination method is required before functionalization. In general, there are two strategies for delaminating LDH compounds, namely the "bottom-up" approach and the "top-down" approach.[1] For the bottom-up synthesis, LDH products are typically prepared *via* a microemulsion-mediated hydrothermal synthesis. The size of the particles can be controlled both in diameter and thickness by tuning the water to surfactant ratio in different reverse microemulsion systems.[37–44] In parallel, significant efforts have focused on the delamination of LDHs by the top-down synthesis in polarized solvents, such as butanol,[45–47] acrylates,[10] formamide[48–52] and *N*,*N*-dimethylformamide–ethanol mixture,[53–55] as well as in nonpolarized solvents such as CCl_4,[56–58] and other type of solvents.[59,60] Adachi-Pagano *et al.*[45] reported the complete delamination of the Zn–Al-LDH using sodium dodecyl sulfate (SDS) as an anionic surfactant and butanol as the dispersant. Ma *et al.*[61] exfoliated Co–Fe-LDHs into nanosheets in formamide by an ultrasonic treatment through hexamethylenetetramine (HMT) hydrolysis. Wu *et al.*[62] reported the direct delamination of Mg–Al–NO_3 in formamide using an ultrasonic treatment at room temperature. The obtained delaminated LDH products in these reports are generally unilamellar sheets. However, for the use in applications, such as catalysis, sensing and electrochemical energy storage devices, designing appropriate client–substrate interactions for the functionalized LDH products is more important to obtain the desired physicochemical properties.[63–65] To this end, unconventional curved LDHs could provide a higher surface area, metal dispersion, suitable morphological structure, reduction properties, and porosity,[66] which would of course increase the accessibility to both the internal galleries and the outer surface, compared with typical plane LDHs.[67–72]

Several reports have synthesized non-conventional LDH morphologies and found that they exhibit interesting sensing,[73] catalytic,[74] photocatalytic,[75] and supercapacitive[76–79] performances. Adachi-Pagano *et al.*[80] reported a sand-rose morphology of Mg–Al-LDHs using a urea hydrolysis method in a mixture solvent of water and ethylene glycol (EG). The size distribution of the mono-dispersed particles was determined by the water/EG ratio, urea concentration and Mg/Al ratio. The preferential adsorption of EG on the (00*l*) planes of Mg–Al-LDH prevents growth in the direction perpendicular to the layers, leading to the inhibition of particle ripening and resulting in the as-obtained sand-rose morphologies. The same phenomenon was observed by Wei *et al.*[81] when synthesizing Li–Al-LDHs using the urea method in a water–ethanol mixture solvent, where the Ostwald ripening mechanism was employed to elucidate the formation of the polymorphic morphologies. The petal-like Li/Al LDHs showed a much higher specific capacitance compared with the spiral structure and hexagonal nanosheets. Using chitosan as a template, Li and coworkers[82] suggested that the Ni–Al-LDH particles co-precipitated through the urea method curves in the *a* direction, while the growth in both the *a* and *c* directions will be inhibited, resulting in a curved fibre-like shapes of the products. Liu *et al.*[65] reported special nanocone structures of Co–M-LDHs (M = Ni, Cu, Zn) using the urea method and simultaneously intercalated dodecyl sulfate (DS) into the interlayer spaces. The LDH nanocones with controllable transition-metal compositions, peculiar hollow feature and large interlayer spacing, exhibited high specific capacitance and remarkable cycling stability when used as supercapacitor electrodes.

China University of Geosciences Wuhan, Wuhan, Hubei, China. E-mail: cgzhou@cug.edu.cn; wujp@cug.edu.cn

We have already mentioned that the polymorphic structural features of different LDH compounds generally occur with the urea method, and that third-party agents, either organic solvents or surfactants, play an important role in forming the special spatial configuration. In fact, these third-party agents should act as an inhibitor to slow down the growth at certain lattice directions or to prevent the particles from agglomerating. Recently, Yan *et al.*[83] reported a one-pot approach to assemble Mg–Al-LDH nanosheets using the urea method, where peroxide was selected as the third-party agent. Within an autoclave environment, the prepared LDH appeared as unilamellar flat nanosheets, and delamination was concluded to be implemented by the oxygen gas from the peroxide decomposition. In the present study, we implemented this one-pot process under ambient pressure within a reflux system. Interestingly, unlike in the sealed system, our procedure offered the opportunity to tune the polymorphic features of Mg–Al-LDH products by changing the peroxide concentration. In particular, with a 20 wt% addition of H_2O_2, curved or even cross-linked delaminated sheets were observed. Based on the XRD, SEM, FT-IR and TGA characterizations, we proposed a different concerted growth mechanism to explain the as-obtained curved patterns, which might be useful for understanding the synthesis of different morphologies for similar hydroxide systems.

Experimental

Preparation of the materials

All analytical-grade chemicals utilized in our experiments were used as purchased. The Mg^{2+}, Al^{3+} precursors (as $Mg(NO_3)_2 \cdot 6H_2O$, $Al(NO_3)_3 \cdot 9H_2O$, respectively) and urea were dissolved in deionized water or peroxide solution in a 500 mL round-bottom flask with a $Mg^{2+} : Al^{3+}$: urea molar ratio of 4 : 1 : 10 at room temperature, where the Mg^{2+} concentration was set to 0.004 mol L^{-1}. The following co-precipitation process was carried out within the same flask under ambient pressure with reflux. For the water solvent, we considered four bath temperatures (100 °C, 120 °C, 150 °C and 180 °C) and three bath durations (3 h, 5 h and 8 h) to determine the optimal synthesis conditions. These parameters were successively employed for the peroxide solution solvent, where three different peroxide concentrations (10 wt%, 20 wt% and 30 wt%) were studied. The filtered solid products were washed with deionized water five times and then dried at 60 °C for 12 h before characterization.

Characterization techniques

The X-ray diffraction (XRD) data of all the samples were collected on a German Bruker D8-Focus powder X-ray diffractometer with Cu Kα radiation ($\lambda = 1.540598$ Å) at a scanning rate of 0.05 seconds per step. Thermogravimetric analysis was carried out on a TGA-DSC (STA449 F3, NETZSCH, German) instrument, where the temperature range was set to 30–1000 °C at a heating rate of 10 °C min^{-1} under N_2 atmosphere. Fourier-transform infrared (FT-IR) spectra were recorded with a Fisher Nicolet 6700. Scanning electron microscopy (SEM) was performed on a Hitachi D8-Focus instrument at an acceleration voltage of 0.1–30 kV.

Results and discussion

We first characterized the LDH samples prepared in water solvent at different temperatures, where the synthesis duration was set to 8 h. The XRD patterns are shown in Fig. 1. At the temperature of 100 °C, no observable diffraction peak can be observed, indicating the products may appear as an amorphous state. As the bath temperature increases to 120 °C and 150 °C, typical diffraction peaks at low angles as indexed by (003), (006), (009) and at high angles for (110), (113) in the XRD patterns suggest the lamellate layers are well crystallized. However, if the bath temperature is set too high (180 °C in our experiments), the crystalline behaviour is considerably weakened. According to the chemical properties of the precursors we used, we can conclude that the major reason for the observed crystalline behaviour is due to the hydrolysis/decomposition of urea. Since the LDH nucleation process occurs in a water or water–peroxide environment, where the temperature variation is limited at different bath temperature, the detailed composition of the as-obtained LDH products should be approximated,[84,85] leading to the typically observed XRD patterns of Mg–Al–CO_3 LDHs as reported previously.[35,86] On the other hand, at the liquid–gas interface, the boiled species may be over-heated by the bath and the reflux system will then recycle the agents. At relatively low temperatures, urea hydrolysis plays the dominant role and provides –OH species for the co-precipitation. The increased bath temperature accelerates the hydrolysis kinetics, leading to better crystalline features. Over-heating the liquid/gas phase results in the decomposition of both the peroxide and urea to generate O_2 and –NCO species, as well as –OH production might be lowered. Therefore, a high bath temperature is not beneficial for the crystalline behaviour. In addition, the top two XRD patterns, which belong to the duration of 3 h and 5 h at 150 °C,

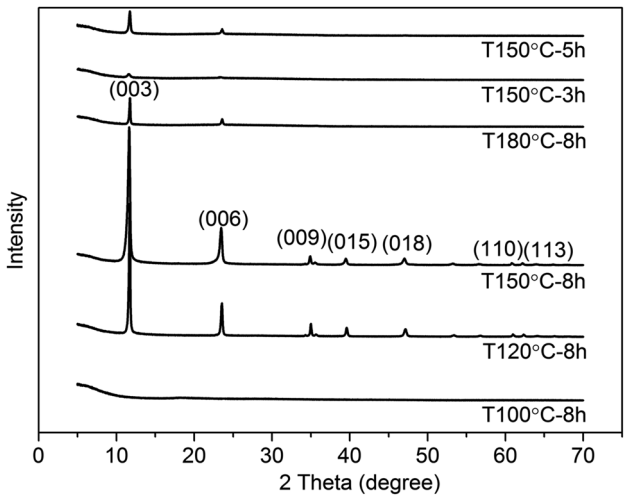

Fig. 1 XRD patterns of LDH samples prepared at different bath temperatures and durations: 100 °C 8 h, 120 °C 8 h, 150 °C 8 h, 180 °C 8 h, 150 °C 3 h and 150 °C 5 h.

indicate that the reaction duration is also essential to the LDH crystallization. Consequently, we assigned 150 °C and 8 h as the optimal conditions in our subsequent studies.

Similar to the report by Yan *et al.*[83] herein, we utilized different peroxide–water mixers as the solvent (with the peroxide ratios of 10 wt%, 20 wt% and 30 wt%, and denoted the products as LDH-P10, LDH-P20, LDH-P30, respectively) to carry out the one-pot co-precipitation of Mg–Al-LDH in the same ambient-pressure reflux system. Fig. 2 displays the XRD patterns of the three samples, as well as the optimal sample prepared at 150 °C for 8 h (denoted by LDH-W) for comparison purposes. Moreover, under the same conditions, the introduction of peroxide led to considerable structural changes of LDH. As the peroxide concentration increased, the LDH feature peaks gradually diminished and then vanished as the H_2O_2 concentration reached 30 wt%. In general, the weakening of the peaks (003) and (006) should be an unambiguous clue for the degree of LDH delamination.[76] In accordance with the SEM characterizations shown in Fig. 3a, uniform and round-shaped LDH sheets can be obtained in water solvent in the ambient-pressure reflux system, with a mean sheet size of 2 μm and a thickness of about 30 nm. The addition of peroxide resulted in a general decrease in the LDH size. At 10 wt% (Fig. 3b), the lateral sizes of the LDH-P10 nanosheets were around 0.5 μm, while the thickness of the sheets decreased to about one-third of LDH-W, implying that the LDH was partially delaminated. Once the peroxide concentration was adjusted to 20 wt% (Fig. 3c1), both the particle size and thickness shrank slightly, with the XRD features suggesting that the delamination degree was improved. The major difference between these two peroxide concentrations is that a lower peroxide addition led to a slight edge bending of the sheets, while a higher peroxide addition resulted in a severe distortion of the planar sheets. Part of the heavily curved fragments even cross-linked, and thus formed a petal-like morphology, as shown in Fig. 3c2. As we increased the peroxide ratio to 30 wt% (Fig. 3d), both the vanished XRD peaks

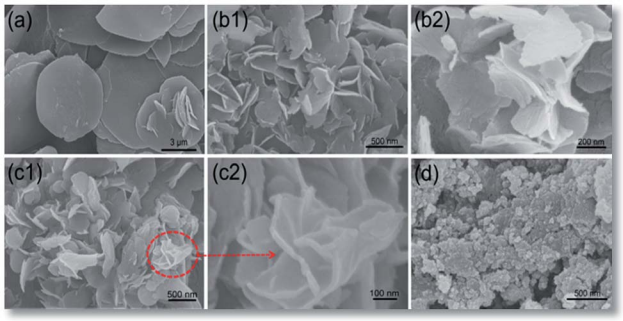

Fig. 3 The SEM image of the samples: (a) LDH-W, (b) LDH-P10, (c) LDH-P20 and (d) LDH-P30.

and the amorphous SEM morphologies of the sample suggest that the crystalline structure could not be assembled.

As seen in Fig. 4 and Table 1, for the standard Mg–Al-LDH products, there are two distinct weight loss stages within the temperature ranges of 30–232.5 °C and 232.5–500 °C.[87,88] The first stage (S1) corresponds to the evaporation of the physically adsorbed water molecules around the particle shell and the intercalated water molecules, while the second stage (S2) is ascribed to the thermal decomposition of carbonate groups and the conversion of hydroxide to oxide. As shown in Fig. 4, the weight loss behaviours of the four samples in both the two stages exhibit an apparent dependence with respect to the concentration of the peroxide. Compared with LDH-W, both the S1 and S2 weight losses decrease when the amount of H_2O_2 added is below 20 wt%, which leads to shrinking particle sizes and weakened LDH crystalline feature, as elucidated by the XRD and SEM results. Herein, we mentioned that for the 10 wt% and 20 wt% amounts of peroxide added, the TG curves vary only slightly. While for LDH-P30, the S1 weight loss is the highest due to the strong amorphous morphology and smallest particle sizes, which provide more sites for physisorbing water molecules. Such a non-crystalline feature implies that the abundance of intercalated carbonate groups is lower than in the other three

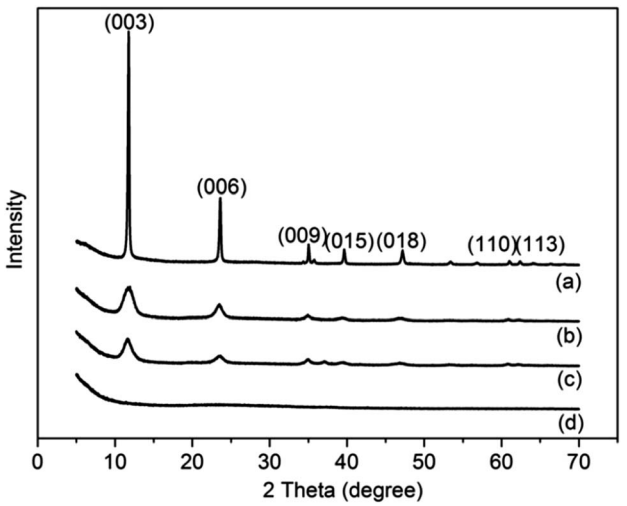

Fig. 2 The XRD patterns of four resultant materials: (a) LDH-W, (b) LDH-P10, (c) LDH-P20 and (d) LDH-P30.

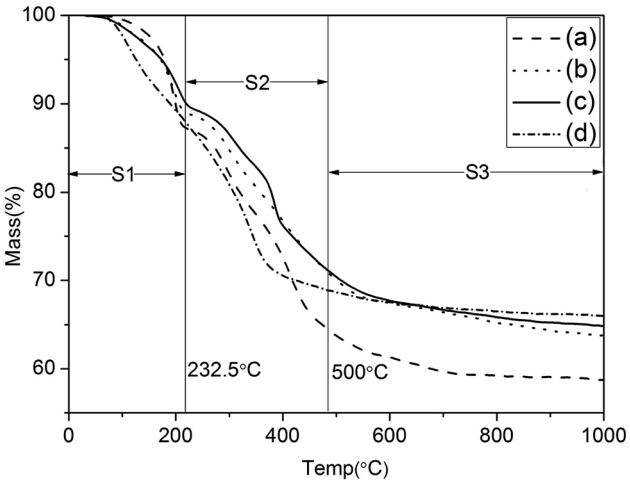

Fig. 4 TG curves of the Mg–Al–CO_3 LDH samples: (a) LDH-W, (b) LDH-P10, (c) LDH-P20 and (d) LDH-P30.

Table 1 The weight loss of two stages for the four samples

Sample	S1 (30–232.5 °C)	S2 (232.5–500 °C)	S3 (500–1000 °C)
(a) LDH-W	13.08%	23.18%	5.00%
(b) LDH-P10	11.32%	18.68%	6.21%
(c) LDH-P20	10.56%	19.04%	5.58%
(d) LDH-P30	13.17%	18.17%	2.64%

cases, and the S2 weight loss should mainly be attributed to the hydroxide decomposition. Beyond 500 °C, the low weight loss of LDH-P30 is the highest due to its non-crystalline nature. For the other three samples, the weight loss of S3 belongs to the final conversion of hydroxides to oxides, along with the deconstruction of the sheet structures.

The FT-IR spectra shown in Fig. 5 suggest that the absorption at 3460 cm^{-1}, which belongs to the –OH stretching of the intercalated and absorbed water molecules, was observed for all the four samples. Three peaks at 3080 cm^{-1}, 1357 cm^{-1} and 691 cm^{-1}, associated with the hydrogen bonding of the water–carbonate, symmetric stretching and translational mode of carbonate, respectively, are present except for LDH-P30, which is consistent with our analysis from the TG measurements. Due to the amorphous nature of LDH-P30, the translation modes of hydroxyl ions associated with trivalent aluminium peak at 774 cm^{-1} and 556 cm^{-1} also vanished. In addition, the absorption band at around 1389 cm^{-1} can be assigned to the characteristic diffraction peaks of the intercalated nitrate groups, which appear only in LDH-P30. Interestingly, a non-negligible peak at 984 cm^{-1}, which can be assigned to the deformation modes of the –OH groups[89] connected with Al^{3+}, was observed for all the samples prepared with the addition of peroxide, but was invisible for the sample of LDH-W assembled in pure water solvent. This motivated us to speculate whether the curling or amorphous nature of the LDH-P series might be connected to this unexpected peak, and consequently led us to deduce the growing mechanism that governs the assembly of the LDH-P samples.

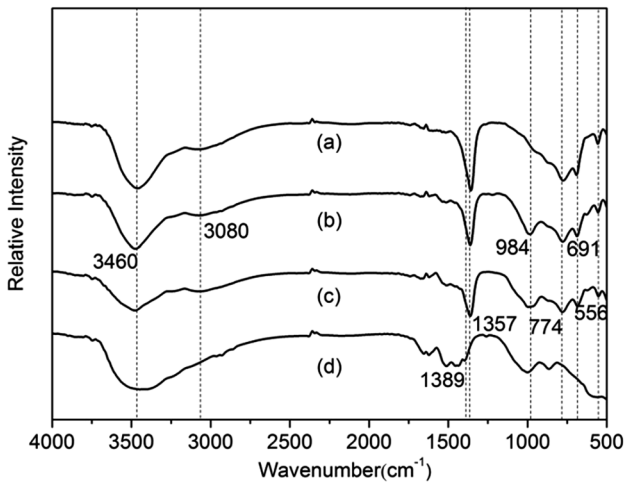

Fig. 5 FT-IR spectra of LDH samples: (a) LDH-W, (b) LDH-P10, (c) LDH-P20 and (d) LDH-P30.

From the periodic model of the Mg–Al-LDH in Fig. 6a, the –OH groups covering on the dual side of the plane all adopt an sp^3 hybridization configuration. In a perfect LDH plane, each –OH connects three-foldedly with metal cations, and each cation attaches with three hydroxyl groups. At the Al^{3+} sites, extra carbonate groups should reside nearby to balance the charge. Such a configuration provides strong restriction to the –OH deformation and makes each single layer a flat plane. The appearance of the peak at 984 cm^{-1} suggests that the –OH deformation around Al^{3+} has been unlocked for LDH-P10, LDH-P20 and LDH-P30. In accordance with the curved or amorphous morphologies, this implies the existence of point defects in the LDH plane. Considering the fact that the hydrolysis of urea is the major source of the hydroxyl group, adding peroxide should lower –OH production, which would slow down the crystalline process to a certain degree. On the other hand, the decomposition of peroxide generates large amounts of oxygen gas, which should provide the driving force for the delamination.[83] Herein, we mentioned that the peroxide decomposition and LDH co-precipitation in fact occur simultaneously, which implies that the delamination of large LDH particles might not be realistic.

Instead, we proposed that, when peroxide participates in the reaction, the growth of the LDH-P10, LDH-P20 and LDH-P30 samples should follow a concerted pathway, which combines peroxide decomposition and LDH co-precipitation. Under such a condition, the generated O_2 would prevent the particles from being ripened. Once a certain amount of nuclei are formed, the growth then prefers to cumulate at the plane edge rather than aggregating with the adjacent particles. Within this locally gaseous environment, –OH defects have a certain probability to appear during co-precipitation, and the remaining charges are

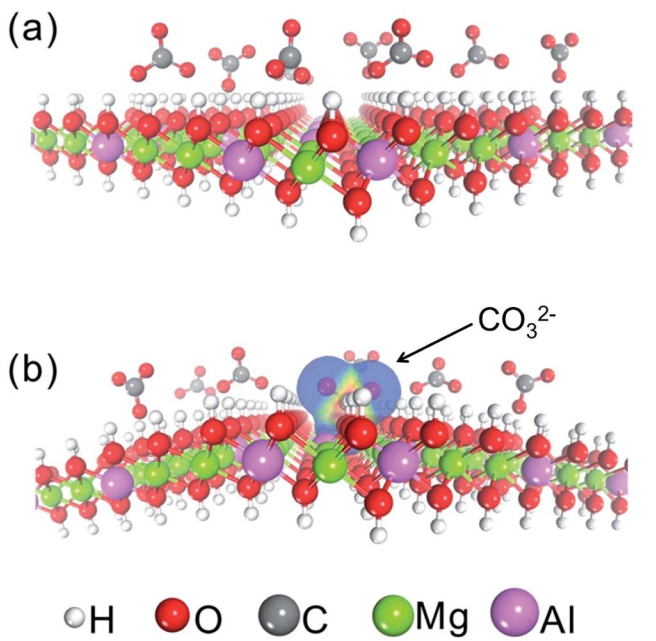

Fig. 6 Schematic illustration of (a) perfect Mg–Al-LDH slab and (b) defective Mg–Al-LDH slab with the defect compensated by the carbonate group. The white, red, grey, green and pink atoms stand for the H, O, C, Mg and Al atoms, respectively.

compensated by carbonate groups generated from the urea decomposition. Compared with a perfect Mg–Al-LDH slab (Fig. 6a), the chemically attached carbonate groups at the –OH defects are repulsive to the –OH groups nearby. Such repulsion forces the planar slab to curve in order to release the intrinsic stress, as illustrated by Fig. 6b. Due to their chemically bonded nature, the thermal stability of carbonate groups should be a little bit higher, as evidenced by the higher thermal decomposition temperatures of carbonate in the TG curves in Fig. 4. Simultaneously, the slight blue-shift of the carbonate feature peaks shown in Fig. 5 is also a clear clue for such a compensation form instead of the traditional intercalated carbonate form. Finally, if the peroxide is in excess, a high O_2 production would heavily influence the co-precipitation and result in small cross-linked fragments or an amorphous state. In fact, these unusual morphologies of LDH products are mostly observed when using the urea method as the precipitator.[65,80–82] We believe that the proposed concerted growth mechanism for explaining the curved morphology in our experiments can be also employed to elucidate those atypical growth phenomena.

Conclusions

We implemented a simple one-pot procedure for assembling Mg–Al–CO_3 LDH through a co-precipitation method within a reflux system under atmospheric pressure. Using water as a dispersing medium, typical uniform LDH sheets can be obtained at the optimal bath temperature of 150 °C and at a duration of 8 h. Under such conditions, as peroxide participates in the process, the morphological features of the as-obtained LDH products are determined by the amount of peroxide added. Through XRD and SEM characterization, we noted that not only did the LDH particle size decreased with the increasing peroxide concentration, but the products display curved or even amorphous nature. The clues provided by TGA and FT-IR measurements imply that under the set condition, the assembling of Mg–Al–CO_3 LDH may not adopt a typical crystallization–delamination process as reported previously. In fact, we deduced that a locally gaseous environment created by the O_2 from the peroxide decomposition plays an essential role for generating the curved or amorphous morphologies. Besides the function that prevents the particles from being aggregated, –OH point defects also occur and the net charges are compensated by carbonate groups, leading to a defective configuration and presenting a curved sheet or amorphous state.

Acknowledgements

The study was supported by the Fundamental Research Founds for National University, China, the University of Geosciences (Wuhan) ("Tengfei" plan, Grant. CUG110501; Innovative Team, Grant CUG120115), and the Natural Science Foundation of Hubei (Grant 2013CFB413 and 2011CDA070).

References

1 Q. Wang and D. O'Hare, *Chem. Rev.*, 2012, **112**, 4124.
2 D. G. Evans and R. C. T. Slade, *Struct. Bonding*, 2006, **119**, 1.
3 A. I. Khan, A. Ragavan, B. Fong, C. Markland, M. O'Brien, T. G. Dunbar, G. R. Williams and D. O'Hare, *Chem. Rev.*, 2009, **48**, 10196.
4 A. I. Khan and D. O'Hare, *J. Mater.*, 2002, **12**, 3191.
5 P. Benito, M. Herrero, F. M. Labajos and V. Rives, *Appl. Clay Sci.*, 2010, **48**, 218.
6 F. Cavani and F. Trifirò, *Catal. Today*, 1991, **11**, 173.
7 J. He, M. Wei, B. Li, Y. Kang, D. G. Evans and X. Duan, *Struct. Bonding*, 2006, **119**, 89.
8 G. R. Williams, A. I. Khan and D. O'Hare, *Struct. Bonding*, 2006, **119**, 161.
9 R. Z. Ma and T. Sasaki, *Adv. Mater.*, 2010, **22**, 5082.
10 S. O'Leary, D. O'Hare and G. Seeley, *Chem. Commun.*, 2002, 1506.
11 L. Z. Qiu, W. Chen and B. J. Qu, *Polym. Degrad. Stab.*, 2005, **87**, 433.
12 L. Li, R. Z. Ma, Y. Ebina, N. Iyi and T. Sasaki, *Chem. Mater.*, 2005, **17**, 4386.
13 D. P. Yan, J. Lu, M. Wei, J. B. Han, J. Ma, F. Li, D. G. Evans and X. Duan, *Angew. Chem., Int. Ed.*, 2009, **48**, 3073.
14 E. P. Landman and W. W. Focke, *S. Afr. J. Sci.*, 2006, **102**, 581.
15 Y. Z. Bao, L. F. Cong, Z. M. Huang and Z. X. Weng, *J. Mater. Sci.*, 2008, **43**, 390.
16 A. R. Wang, Y. Z. Bao, Z. X. Weng and Z. M. Huang, *Chin. J. Chem. Eng.*, 2008, **16**, 938.
17 D. Sudha and A. Ramasubbu, *Asian J. Chem.*, 2013, **25**, S120.
18 F. Leroux and J. P. Besse, *Chem. Mater.*, 2001, **13**, 3507.
19 Q. Z. Yang, D. J. Sun, C. G. Zhang, X. J. Wang and W. A. Zhao, *Langmuir*, 2003, **19**, 5570.
20 M. S. Cho, B. Shin, S. D. Choi, Y. Lee and K. G. Song, *Electrochim. Acta.*, 2004, **50**, 331.
21 J. Tronto, F. Leroux, M. Dubois, J. F. Borin, C. F. de Oliveira Graeff and J. B. Valim, *J. Phys. Chem. Solids*, 2008, **69**, 1079.
22 R. Gao, M. J. Zhao, Y. Guan, X. Y. Fang, X. H. Lia and D. P Yan, *J. Mater. Chem. C*, 2014, **2**, 9579.
23 H. Y Ma, R. Gao, D. P. Yan, J. W. Zhao and M. Wei, *J. Mater. Chem. C*, 2013, **1**, 4128.
24 J. M. Oh, S. Y. Kwak and J. H. Choy, *J. Phys. Chem. Solids*, 2006, **67**, 1028.
25 M. J. Masarudin, K. Yusoff, R. A. Rahim and M. Z. Hussein, *Nanotechnology*, 2009, **20**, 045602.
26 A. L. McKenzie, C. T. Fishel and R. J. Davis, *J. Catal.*, 1992, **138**, 547.
27 B. Sels, D. D. Vos, M. Buntinx, F. Pierard, A. K. de Mesmaeker and P. Jacobs, *Nature*, 1999, **400**, 855.
28 B. Yang and Z. H. Yang, *RSC Adv.*, 2013, **3**, 12589.
29 M. Sebastian, C. Nethravathi and M. Rajamathi, *Mater. Res. Bull.*, 2013, **48**, 2715.
30 J. Han, K. C. Roh, M. R. Jo and Y. M. Kang, *Chem. Commun.*, 2013, **49**, 7067.
31 X. M. Fan, Z. H. Yang, R. J. Wen, B. Yang and W. Long, *J. Power Sources*, 2013, **224**, 80.
32 A. B. Béléké, E. Higuchi, H. Inoue and M. Mizuhata, *J. Power Sources*, 2013, **225**, 215.
33 J. W. Zhao, J. Chen, S. Xu, M. F. Shao, D. P. Yan, M. Wei, D. G. Evans and X. Duan, *J. Mater. Chem. A*, 2013, **1**, 8836.

34 D. P. Yan, J. Lu, J. Ma, M. Wei, D. G. Evans and X. Duan, *Angew. Chem., Int. Ed.*, 2011, **50**, 720.
35 D. P. Yan, Y. B. Zhao, M. Wei, R. Z. Liang, J. Lu, D. G. Evans and X. Duan, *RSC Adv.*, 2013, **3**, 4303.
36 A. M. Bashi, S. M. Haddawi and M. A. A. Mezaal, *Arabian J. Sci. Eng.*, 2013, **38**, 1663.
37 G. Hu, N. Wang, D. O'Hare and J. Davis, *Chem. Commun.*, 2006, 287.
38 G. Hu and D. O'Hare, *J. Am. Chem. Soc.*, 2005, **127**, 17808.
39 G. Hu, N. Wang, D. O'Hare and J. Davis, *J. Mater. Chem.*, 2007, **17**, 2257.
40 C. J. Wang, Y. A. Wu, R. M. J. Jacobs, J. H. Warner, G. R. Williams and D. O'Hare, *Chem. Mater.*, 2010, **23**, 171.
41 F. Bellezza, A. Cipiciani, U. Costantino, M. Nocchetti and T. Posati, *Eur. J. Inorg. Chem.*, 2009, **18**, 2603.
42 S. N. Khadzhiev, K. M. Kadiev, G. P. Yampolskaya and M. K. Kadieva, *Adv. Colloid Interface Sci.*, 2013, **197–198**, 132.
43 J. Liang, Y. Y. Ma, H. Sun, W. Li and L. X. Wu, *J. Colloid Interface Sci.*, 2013, **409**, 80.
44 J. Stergar, G. Ferk, I. Ban, M. Drofenik, A. Hamler, M. Jagodič and D. Makovec, *J. Alloys Compd.*, 2013, **576**, 220.
45 M. Adachi-Pagano, C. Forano and J. P. Besse, *Chem. Commun.*, 2000, 91.
46 F. Leroux, M. Adachi-Pagano, M. Intissar, S. Chauviere, C. Forano and J. P. Besse, *J. Mater. Chem.*, 2001, **11**, 105.
47 M. Singh, M. I. Ogden, G. M. Parkinson, C. E. Buckley and J. M. Connolly, *J. Mater. Chem.*, 2004, **14**, 871.
48 F. Wypych, G. A. Bubniak, M. Halma and S. Nakagaki, *J. Colloid Interface Sci.*, 2003, **264**, 203.
49 T. Hibino, *Chem. Mater.*, 2004, **16**, 5482.
50 Z. P. Liu, R. Z. Ma, M. Osada, N. Iyi, Y. Ebina, K. Takada and T. Sasaki, *J. Am. Chem. Soc.*, 2006, **128**, 4872.
51 Z. P. Liu, R. Z. Ma, Y. Ebina, N. Iyi, K. Takada and T. Sasaki, *Langmuir*, 2006, **23**, 861.
52 J. B. Liang, R. Z. Ma, N. Iyi, Y. Ebina, K. Takada and T. Sasaki, *Chem. Mater.*, 2009, **22**, 371.
53 Y. Zhao, W. D. Yang, Y. H. Xue, X. G. Wang and T. Lin, *J. Mater. Chem.*, 2011, **21**, 4869.
54 R. L. Frost, J. Kristof, E. Horvath and J. Kloprogge, *J. Phys. Chem. A*, 1999, **103**, 9654.
55 S. Letaief and C. Detellier, *J. Mater. Chem.*, 2005, **15**, 4734.
56 M. Jobbágy and A. E. Regazzoni, *J. Colloid Interface Sci.*, 2004, **275**, 345.
57 W. Y. Tseng, J. T. Lin, C. Y. Mou, S. Cheng, S. B. Liu, P. P. Chu and H. W. Liu, *J. Am. Chem. Soc.*, 1996, **118**, 4411.
58 V. V. Naik, T. N. Ramesh and S. Vasudevan, *J. Phys. Chem. Lett.*, 2011, **2**, 1193.
59 J. Gaume, S. Therias, F. Leroux, A. Rivaton and J. L. Gardette, *J. Appl. Polym. Sci.*, 2013, **129**, 1345.
60 X. H. Liu, R. Z. Ma, Y. Bando and T. Sasaki, *Angew. Chem., Int. Ed.*, 2010, **49**, 8253.
61 R. Z. Ma, Z. P. Liu, K. Takada, N. Iyi, Y. Bando and T. Sasaki, *J. Am. Chem. Soc.*, 2007, **129**, 5257.
62 Q. L. Wu, A. Olafsen, O. B. Vistad, J. Roots and P. Norby, *J. Mater. Chem.*, 2005, **15**, 4695.
63 M. Q. Zhao, Q. Zhang, J. Q. Huang and F. Wei, *Adv. Funct. Mater.*, 2012, **22**, 675.
64 L. Wang, Z. H. Dong, Z. G. Wang, F. X. Zhang and J. Jin, *Adv. Funct. Mater.*, 2013, **23**, 2758.
65 X. H. Liu, R. Z. Ma, Y. Bando and T. Sasaki, *Adv. Mater.*, 2012, **24**, 2148.
66 A. Di Fronzo, C. Pirola, A. Comazzi, F. Galli, C. L. Bianchi, A. Di Michele, R. Vivani, M. Nocchetti, M. Bastianini and D. C. Boffito, *Fuel*, 2014, **119**, 62.
67 J. B. Wei, J. Wang, Y. C. Song, Z. S. Li, Z. Gao, T. Mann and M. L. Zhang, *J. Solid State Chem.*, 2012, **196**, 175.
68 Z. P. Xu, L. Li, C. Y. Cheng, R. G. Ding and C. H. Zhou, *Appl. Clay Sci.*, 2013, **74**, 102.
69 Y. Zhou, Y. Kuang, W. Y. Li, Z. L. Chen, M. Megharaj and R. Naidu, *Chem. Eng. J.*, 2013, **223**, 68.
70 B. Li and J. He, *J. Phys. Chem. C*, 2008, **112**, 10909.
71 M. Jobbágy and N. Iyi, *J. Phys. Chem. C*, 2010, **114**, 18153.
72 T. Gomez, E. Florez, J. A. Rodriguez and F. Illas, *J. Phys. Chem. C*, 2011, **115**, 11666.
73 F. T. Zhang, X. Long, D. W. Zhang, Y. L. Sun, Y. L. Zhou, Y. R. Ma, L. M. Qi and X. X. Zhang, *Sens. Actuators, B*, 2014, **192**, 150.
74 R. K. Sahu, B. S. Mohanta and N. N. Das, *J. Phys. Chem. Solids*, 2013, **74**, 1263.
75 S. J. Xia, F. X. Liu, Z. M. Ni, J. L. Xue and P. P. Qian, *J. Colloid Interface Sci.*, 2013, **405**, 195.
76 Q. F. Wang, X. F. Wang, B. Liu, G. Yu, X. J. Hou, D. Chen and G. Z. Shen, *J. Mater. Chem. A*, 2013, **1**, 2468.
77 X. Sun, G. K. Wang, H. T. Sun, F. Y. Lu, M. P. Yu and J. Lian, *J. Power Sources*, 2013, **238**, 150.
78 L. H. Su, Z. W. Song, L. H. Lu and G. L. Pang, *Mater. Res. Bull.*, 2013, **8**, 3636.
79 M. Hu, X. D. Ji, L. X. Lei and X. W. Lu, *Electrochim. Acta*, 2013, **105**, 261.
80 M. Adachi-Pagano, C. Forano and J. P. Besse, *J. Mater. Chem.*, 2003, **13**, 1988.
81 J. B. Wei, Z. Gao, Y. C. Song, W. L. Yang, J. Wang, Z. S. Li, T. Mann, M. L. Zhang and L. H. Liu, *Mater. Chem. Phys.*, 2013, **139**, 395.
82 B. Li, J. He, D. G. Evans and X. Duan, *J. Phys. Chem. Solids*, 2006, **67**, 1067.
83 Y. X. Yan, Q. Liu, J. Wang, J. B. Wei, Z. Gao, T. Mann, Z. S. Li, Y. He, M. L. Zhang and L. H. Liu, *J. Colloid Interface Sci.*, 2012, **371**, 15.
84 D. P. Yan, J. Lu, M. Wei, J. Ma, D. G. Evans and X. Duan, *Phys. Chem. Chem. Phys.*, 2009, **11**, 9200.
85 D. P. Yan, J. Lu, M. Wei, J. Ma, D. G. Evans and X. Duan, *Phys. Chem. Chem. Phys.*, 2010, **12**, 15085.
86 X. B. Wang, Z. M. Bai, D. Zhao, Y. P. Chai, M. Guo and J. Y. Zhang, *Mater. Res. Bull.*, 2013, **48**, 1228.
87 M. Dixit, M. Mishra, P. A. Joshi and D. O. Shah, *J. Ind. Eng. Chem.*, 2013, **19**, 458.
88 X. Y. Xu, D. Q. Li, J. Q. Song, Y. J. Lin, Z. Lv, M. Wei and X. Duan, *Particuology*, 2010, **8**, 198.
89 T. Zhang, Q. R. Li, H. Y. Xiao, H. X. Lu and Y. M. Zhou, *Ind. Eng. Chem. Res.*, 2012, **51**, 11490.

